nature geoscience

SUPPLEMENTARY INFORMATION

DOI: 10.1038/NGEO1377

Network of off-axis melt bodies at the East Pacific Rise

J. Pablo Canales[1]*, Helene Carton[2], Suzanne M. Carbotte[2], John C. Mutter[2], Mladen R. Nedimović[3, 2], Min Xu[4], Omid Aghaei[3], Milena Marjanović[2] and Kori Newman[2]

[1] Department of Geology and Geophysics, Woods Hole Oceanographic Institution, Woods Hole, MA 02540, USA.

[2] Lamont-Doherty Earth Observatory, Columbia University, Palisades, NY 10964, USA.

[3] Department of Earth Sciences, Dalhousie University, Halifax, Nova Scotia B3H4J1, Canada.

[4] Massachusetts Institute of Technology-Woods Hole Oceanographic Institution Joint Program in Oceanography, Department of Geology and Geophysics, Woods Hole Oceanographic Institution, Woods Hole, MA 02540, USA.

* Corresponding author. E-mail: jpcanales@whoi.edu

Format: PDF

Size: 29.4 MB

This file includes:

SUPPLEMENTARY TABLES (1, 2)

SUPPLEMENTARY FIGURES (S1-S9)

© 2012 Macmillan Publishers Limited. All rights reserved.

DOI: 10.1038/NGEO1377

Table 1. Main acquisition parameters during cruise MGL0812	
Vessel	*RV Marcus G. Langseth*
Hydrophone streamers	Number: 4 Spacing: 150 m Length: 6,000 m Number of groups: 468 Group spacing: 12.5 m
Sources	Number: 2 Source separation: 75 m Number of arrays: 2 per source Number of guns: 9 per array Volume: 54 L (3,300 in^3) per source Source interval: alternate every 37.5 m
Recording	Sampling interval: 2 ms Record length: 10,240 ms Format: SEG-D

© 2012 Macmillan Publishers Limited. All rights reserved.

Table 2. 3D processing sequence

3D geometry definition
Binning: 6.25×37.5 m bins
Band-pass filtering: 5-7-200-225 Hz
Spherical divergence correction
Surface-consistent amplitude correction for shot and channel
Offset distribution regularization (flexible binning in cross-line direction): 0.5×bin size for offsets ≤1,662 m; 1.5×bin size for offsets ≥4,587 (linear interpolation offsets in between those values) (Fig. S1).
Resample to 4 ms and 7-s trace length.
Stacking velocity analysis [a]
Normal move-out correction
Stretch and outer mute (muted offset>2,000 m for the AMC events, offset>2,500 m for OAML events).
Stack CMP gathers
Bottom mute of primary seafloor multiple
Two-pass (in-line and cross-line directions) *f-k* domain post-stack time migration
Top mute above seafloor

[a] Processing was oriented towards optimizing imaging of the axial melt lens and a series of off-axis mid-crustal reflectors. Our stacking velocity model does not include a layer for properly stacking the base of seismic layer 2A, which is a wide-angle reflection[1]. Thus the 3D seismic volume obtained from this processing should not be used for interpreting/analyzing layer 2A events or their absence.

[1] Harding, A. J., Kent, G. M., and Orcutt, J. A., A multichannel seismic investigation of upper crustal structure at 9°N on the East Pacific Rise: Implications for crustal accretion. J. *Geophys. Res.* **98**, 13,925-13,944 (1993).

© 2012 Macmillan Publishers Limited. All rights reserved.

DOI: 10.1038/NGEO1377

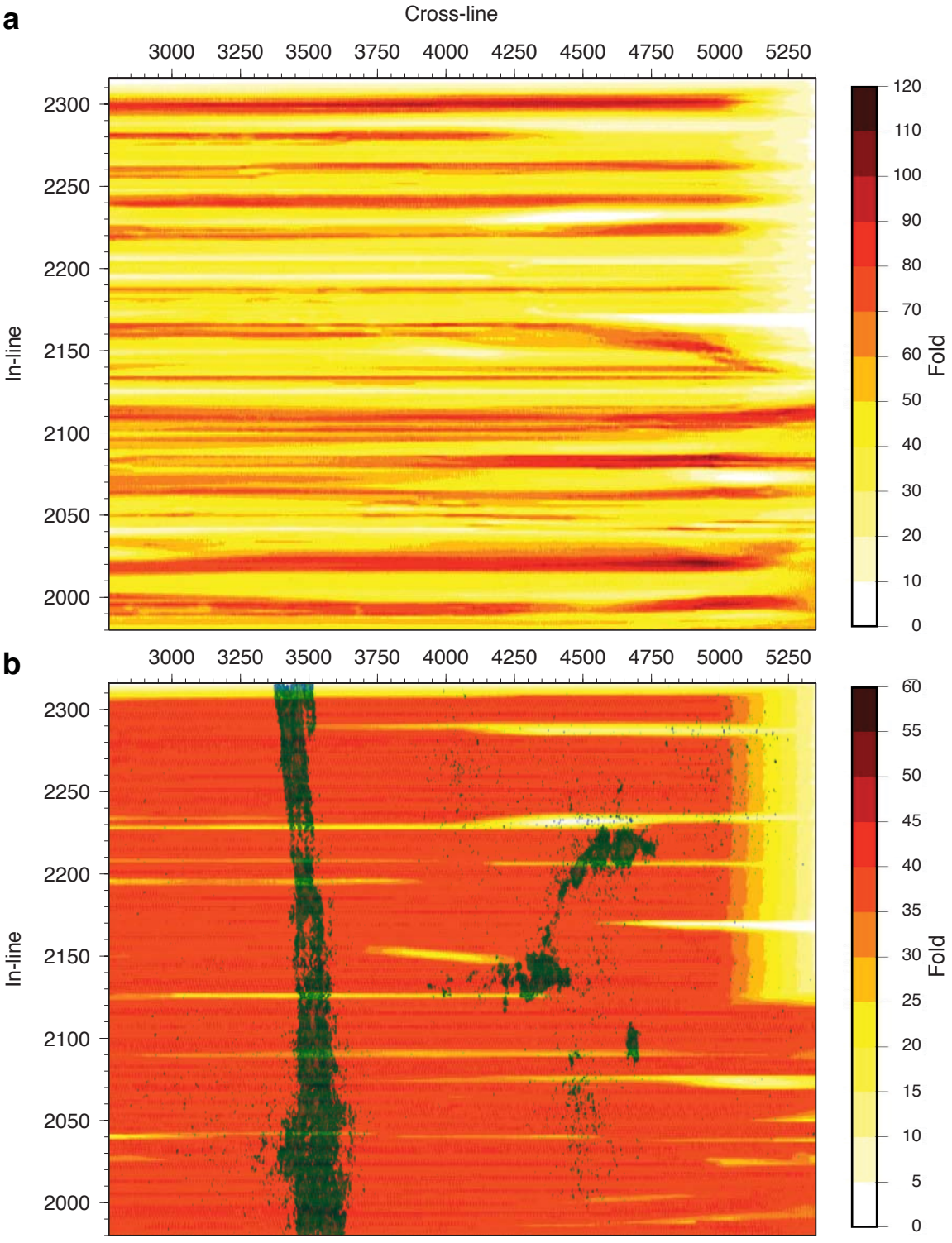

Figure S1. Bin fold maps **a,** before and **b,** after offset distribution regularization. Maximum nominal fold after offset regularization is set to 40. Top-view of the seismic reflectivity of the volume (as in Fig. 2a) has been projected over the fold map.

© 2012 Macmillan Publishers Limited. All rights reserved.

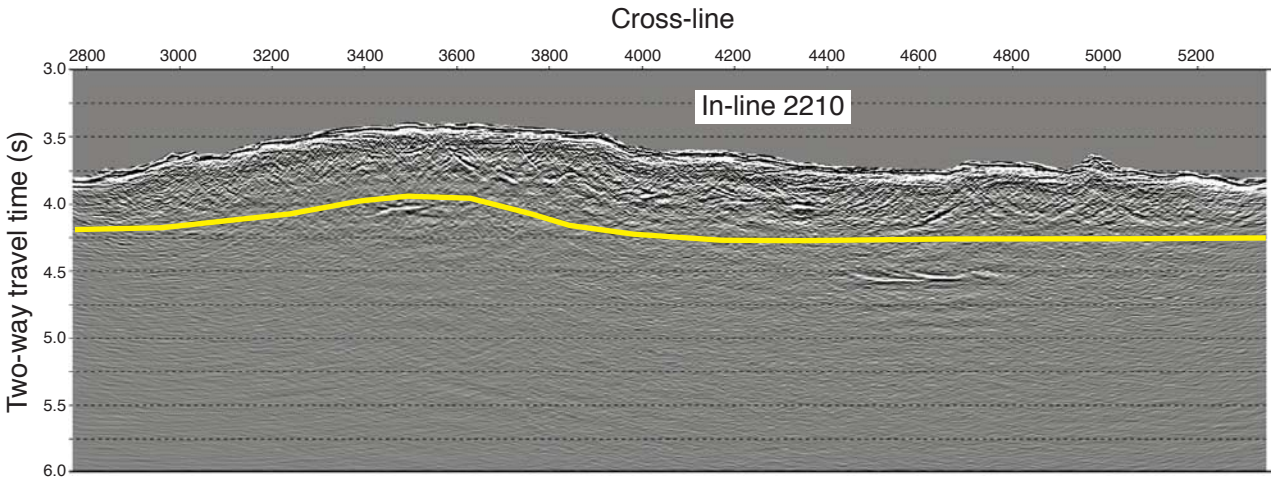

Figure S2. Example of an in-line section showing the top mute (yellow line) applied to the seismic volume prior to calculating the trace energy for 3D visualization of the AMC and OAML events.

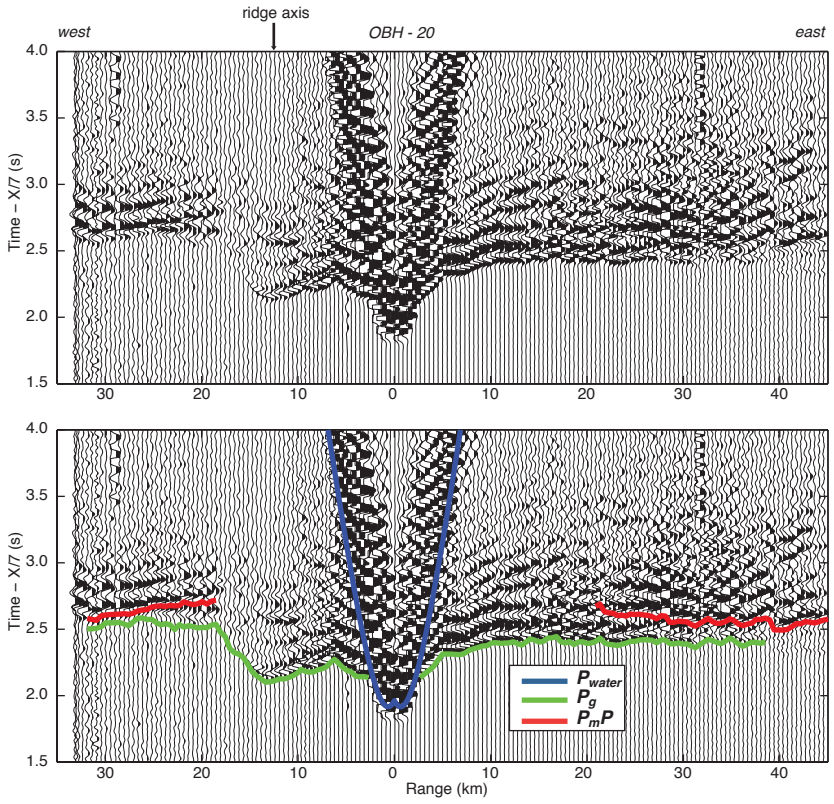

Figure S3. Example of ocean bottom hydrophone record section (top) with main seismic arrivals indicated as colored lines (bottom). Vertical axis is reduced travel time (7 km/s), and horizontal axis is distance between sources and receiver.

© 2012 Macmillan Publishers Limited. All rights reserved.

DOI: 10.1038/NGEO1377

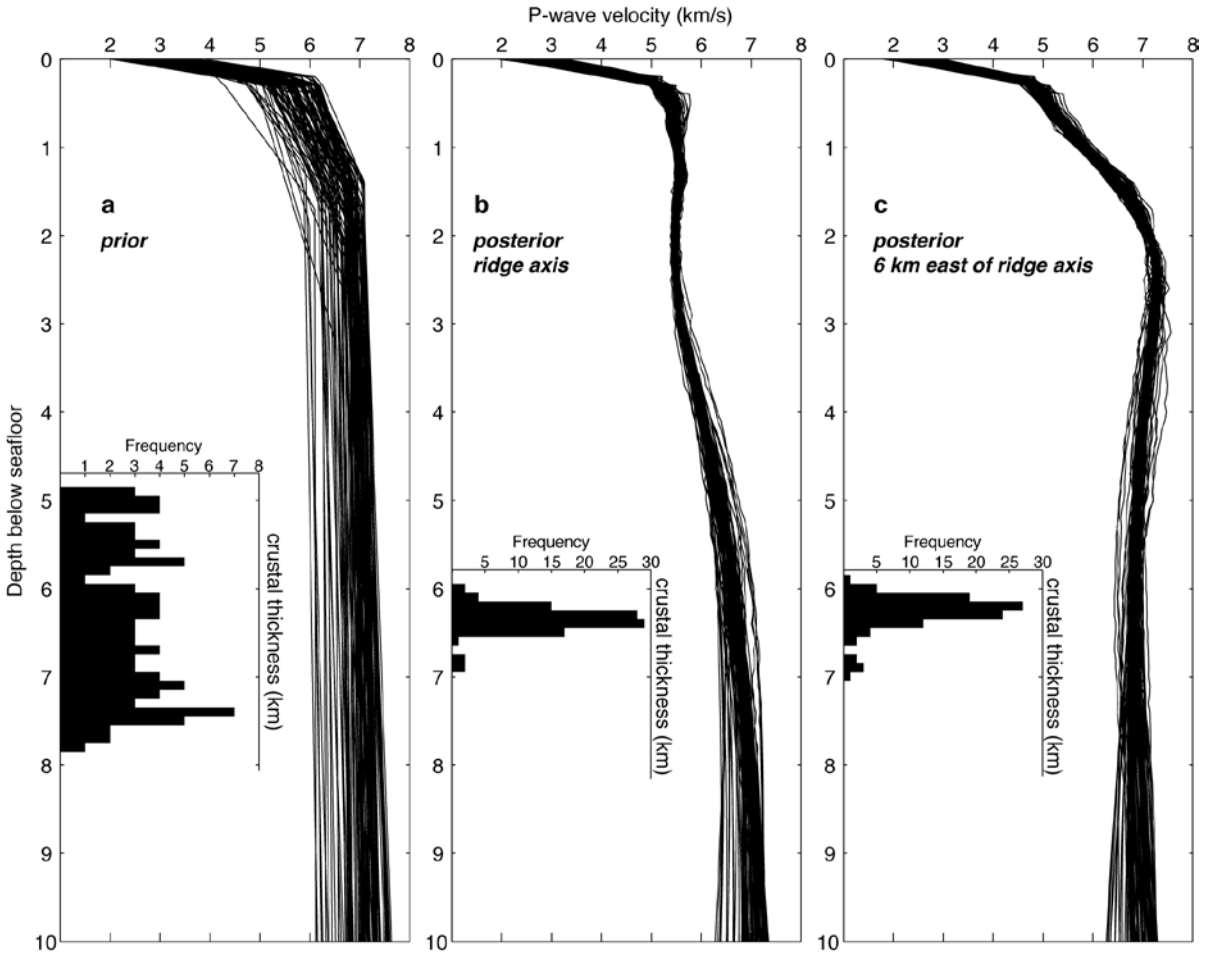

Figure S4. a, Prior 100 random Monte Carlo 1D starting models. **b,** Velocity-depth profiles from the 100 Monte Carlo solutions extracted at the location of the ridge axis. **c,** Velocity-depth profiles from the 100 Monte Carlo solutions extracted 6 km to the east of the ridge axis. Insets with vertical histograms show the distribution of prior and posterior crustal thickness models.

© 2012 Macmillan Publishers Limited. All rights reserved.

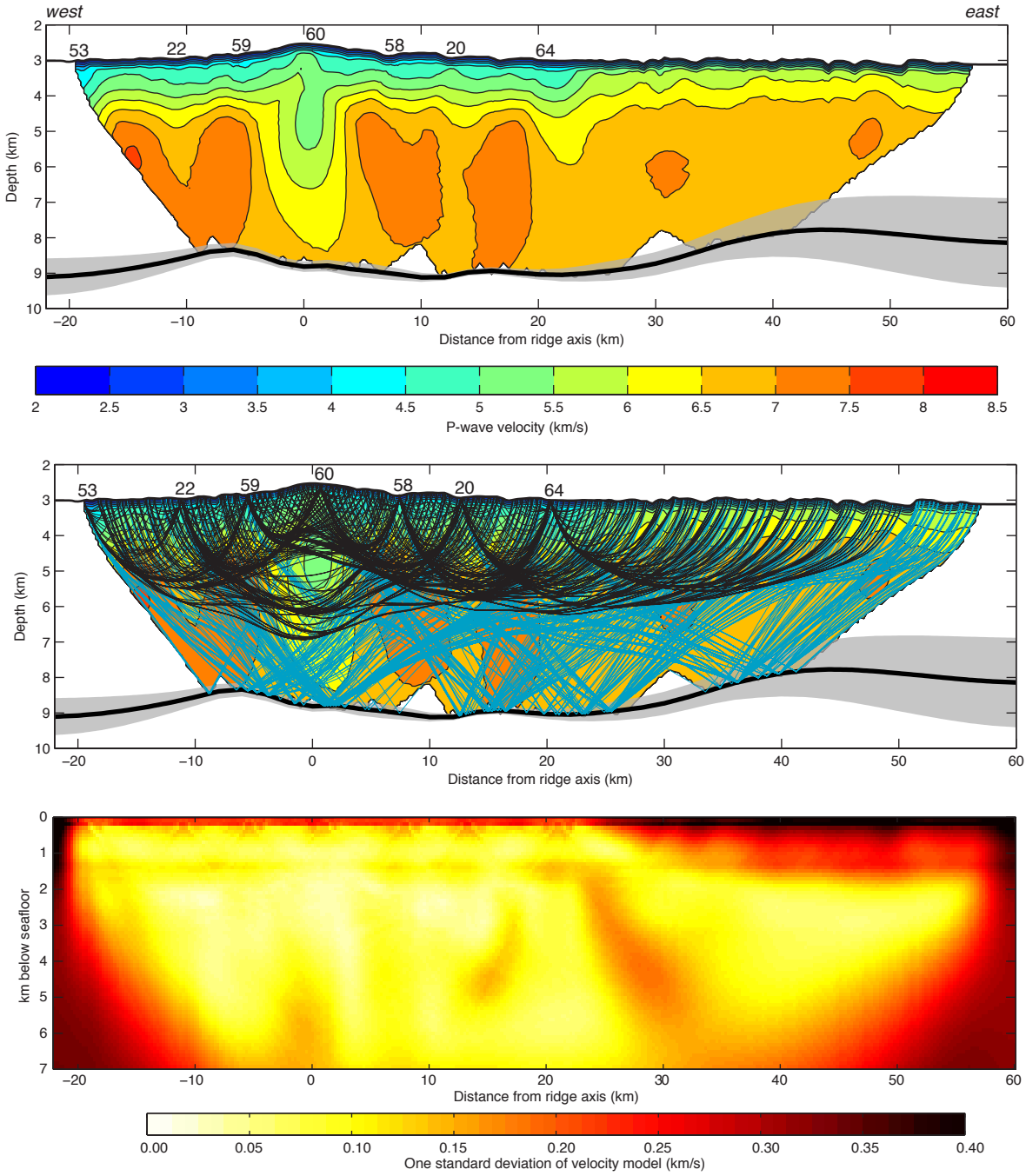

Figure S5. Top: Preferred velocity model (averaged from the 100 Monte Carlo solutions). Only portions of the model constrained by ray paths (middle: black for P_g and blue for P_mP rays) are shown in color. Numbers along bathymetry profile are instrument number. Solid black line is Moho depth (mean of the 100 solutions), and gray bounds show ±1σ. Bottom: One standard deviation map of the 100 Monte Carlo solutions. Note the higher velocity uncertainty in the shallow crust for X>20 km due to lack of recordings along the eastern half of the profile.

© 2012 Macmillan Publishers Limited. All rights reserved.

DOI: 10.1038/NGEO1377

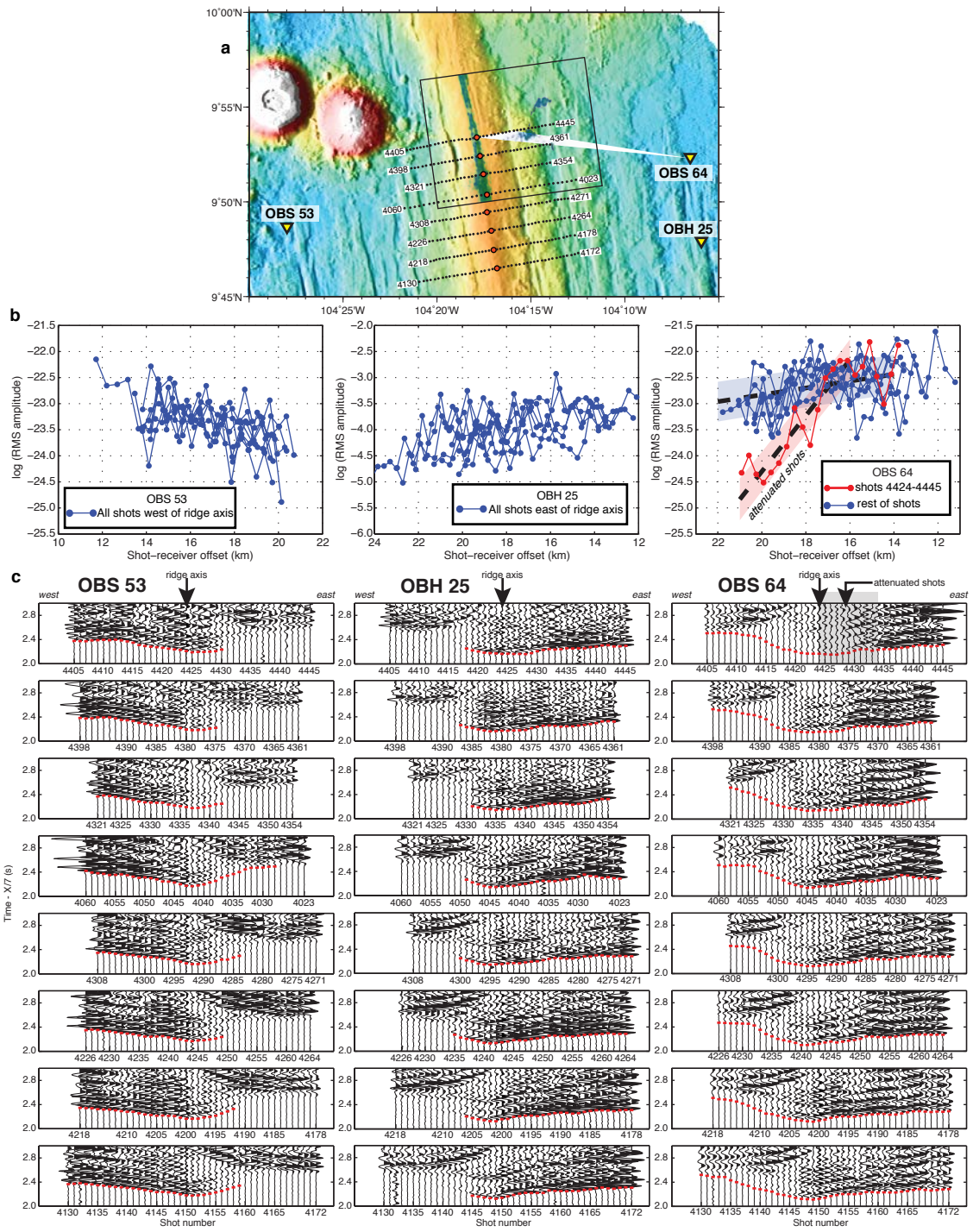

Figure S6. Attenuation analysis of UNDERSHOOT data from instruments OBS 53, OBH 25, and OBS 64. See description of panels and symbols in Fig. 4. Note that, with the exception of shots 4424-4433 recorded by OBS 64, none of the other record sections show evidence of seismic attenuation. This indicates that the attenuation pattern shown in Fig. 4 is a local feature associated with the OAMLs.

© 2012 Macmillan Publishers Limited. All rights reserved.

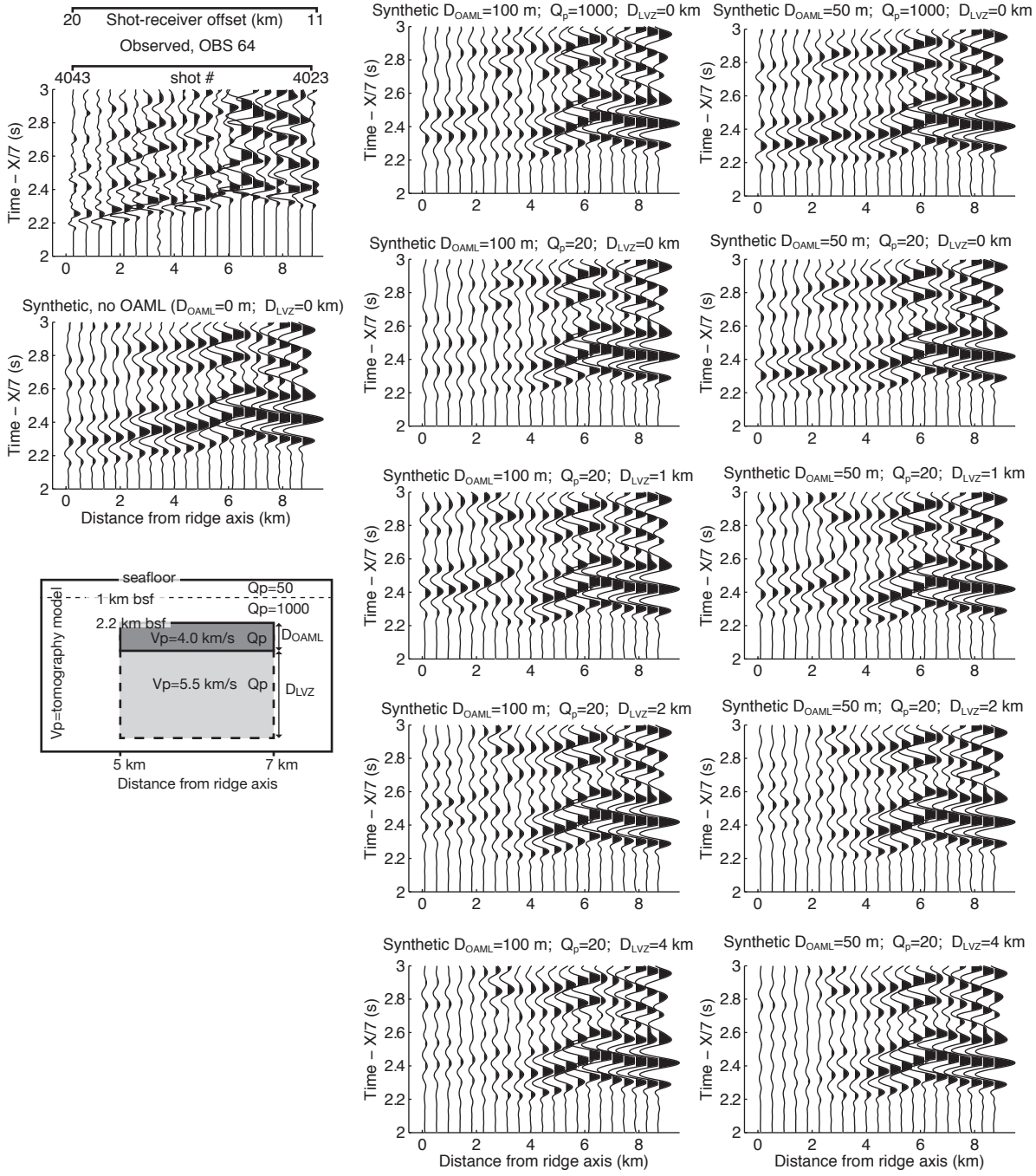

Figure S7. Non-attenuated seismograms from UNDERSHOOT instrument OBS 64 for shots 4023-4043 (Fig. S6) compared to synthetic seismograms calculated for several models with different OAML properties and sub-OAML low velocity volume added to the tomography model of Fig. S5 (diagram). Synthetic seismograms were calculated using a finite-difference approximation of the acoustic wave equation in the frequency domain (Pratt, R. G. & Worthington, M. H. Inverse theory applied to multi-source cross-hole tomography. Part 1: Acoustic wave-equation method. *Geophysical Prospecting* **38**, 287-310 (1990)). Source wavelet is a three-excursion Kupper wavelet with central frequency at 6 Hz, band-pass filtered between 4-5-8-10 Hz to simulate the narrow frequency content of the OBS data. Velocity, density, and attenuation models were discretized at 12.5 m intervals. Synthetic seismograms were calculated for 15 frequency components evenly sampled between 1 and 15 Hz

© 2012 Macmillan Publishers Limited. All rights reserved.

DOI: 10.1038/NGEO1377

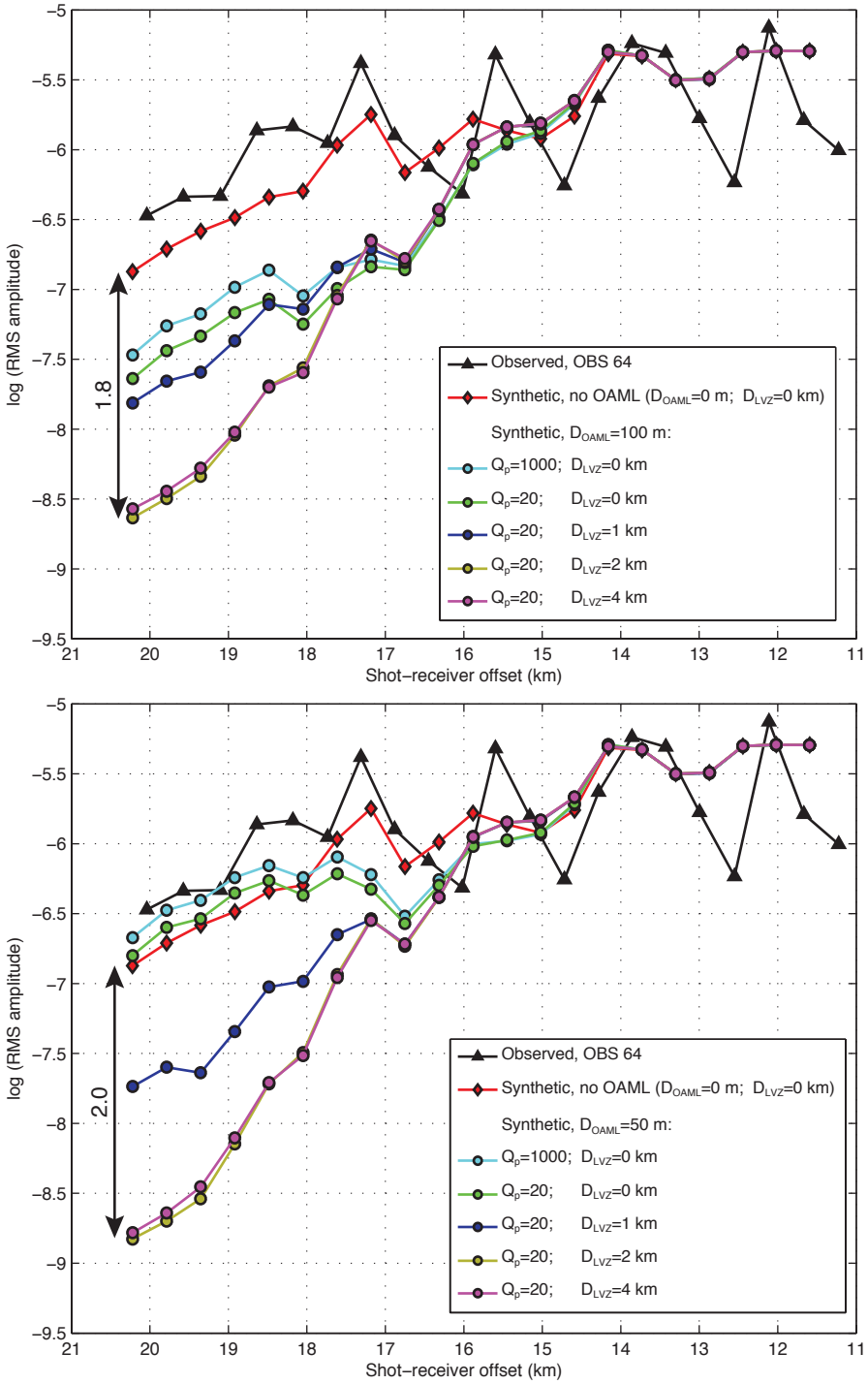

Figure S8. RMS amplitude of first arrivals of the observed and synthetic seismograms shown in Fig. S7. A sub-OAML low velocity volume that is at least 2 km thick produces attenuation in near-ridge seismograms (~20 km offset) of 1.8 natural log units (100-m-thick OAML, top) and 2.0 log units (50-m-thick OAML, bottom), comparable to the 1.9±0.5 natural log units decrease in RMS amplitude observed in ORB-05 data (Fig. 4c).

© 2012 Macmillan Publishers Limited. All rights reserved.

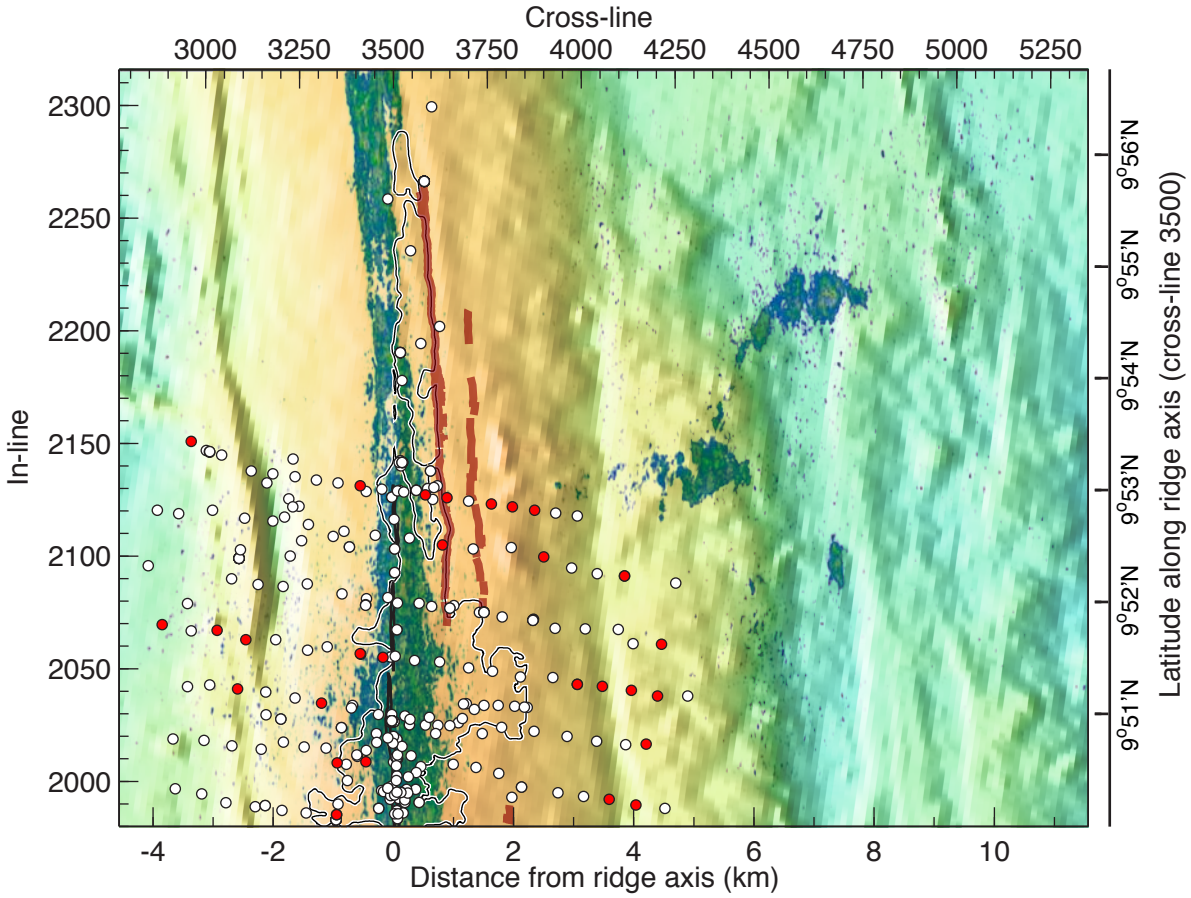

Figure S9. Seismic reflection energy projected over seafloor bathymetry as in Fig. 2b. Circles correspond to locations of existing lava samples that have been analyzed for major element composition (TiO_2 and K_2O). Red and white symbols correspond to enriched and normal compositions, respectively. Enriched composition is defined as wt % $K_2O/TiO_2>0.1$. Data are from the Petrological Database of the Ocean Floor (http://www.petdb.org).

© 2012 Macmillan Publishers Limited. All rights reserved.